



LAWRENCE
LIVERMORE
NATIONAL
LABORATORY

He bubble coarsening by migration and coalescence in annealed Pu-Ga alloys

J. R. Jeffries, M. A. Wall, K. T. Moore, A. J.
Schwartz

October 4, 2010

Journal of Nuclear Materials

Disclaimer

This document was prepared as an account of work sponsored by an agency of the United States government. Neither the United States government nor Lawrence Livermore National Security, LLC, nor any of their employees makes any warranty, expressed or implied, or assumes any legal liability or responsibility for the accuracy, completeness, or usefulness of any information, apparatus, product, or process disclosed, or represents that its use would not infringe privately owned rights. Reference herein to any specific commercial product, process, or service by trade name, trademark, manufacturer, or otherwise does not necessarily constitute or imply its endorsement, recommendation, or favoring by the United States government or Lawrence Livermore National Security, LLC. The views and opinions of authors expressed herein do not necessarily state or reflect those of the United States government or Lawrence Livermore National Security, LLC, and shall not be used for advertising or product endorsement purposes.

He bubble coarsening by migration and coalescence in annealed Pu-Ga alloys

J. R. Jeffries^{a,*} M. A. Wall^a K. T. Moore^a A. J. Schwartz^a

^a*Lawrence Livermore National Laboratory, Livermore, CA 94550, USA*

Abstract

The α -decay of plutonium in Pu-Ga alloys continually generates inert He atoms within the lattice of the Pu-Ga matrix. In naturally aged Pu specimens, those He atoms form into bubbles, He-filled vacancy clusters, with a characteristic size distribution centered near 1.4 nm. Upon annealing, the He bubbles are subject to temperature induced changes in the thermodynamic parameters governing their size, which results in a coarsening of the bubble distribution yielding a lower bubble density but larger average bubble sizes. Herein, we investigate, by means of transmission electron microscopy, the coarsening of He bubbles with several annealing treatments. Micrographs subsequent to the annealing treatments as well as *in situ* observations implicate migration and coalescence as the mechanism for He bubble coarsening with annealing.

Key words: Plutonium, He bubbles, self-irradiation

PACS: 61.82.Bg, 61.72.Cc, 61.72.jd

1. Introduction

The evolution of inert gas bubbles in metals has important implications on the evolution of the mechanical properties of nuclear materials as well as materials in highly irradiating environments, such as those expected in next-generation nuclear reactors [1,2]. With low solubilities in most metals, inert gases accumulate within the lattice as bubbles, the sizes of which are determined by the interfacial surface energy of the bubbles, the degree to which the lattice can accommodate induced strain from the bubbles, and the internal pressure of the bubbles [3]. Internal pressures of He bubbles have been reported to range up to tens of kbar [4,5]. The presence of gas bubbles in metallic lattices can profoundly alter the mechanical properties and strength of materials leading to embrittlement, swelling, and blistering [2,6,7]. These negative consequences are controlled, at least partly, by the thermodynamics and kinetics of bubble formation, growth, and migration, all of which can be strongly temperature dependent [8,9]. The behaviors of gas bubbles are thus important components of any evaluation of the effects of irradiation-induced aging in a material, nuclear or otherwise.

In Pu-Ga alloys composed primarily of ^{239}Pu , He is accumulated at a rate of approximately 41 atomic parts per

million per year through the α decay of the ^{239}Pu isotope [10,11]. This self-irradiating decay process annihilates a Pu nucleus, ejecting two particles into the surrounding lattice: a 5 MeV α particle, which dissipates its energy mostly through heat transferred to the lattice through electronic excitations; and a recoiling, 86-keV ^{235}U nucleus, which dissipates most of its energy through lattice collisions [12]. Those lattice collisions generate thousands of interstitials and vacancies (Frenkel pairs) [13] before the U ion comes to rest, leaving in its wake a damage cascade affecting a volume roughly 15 nm in diameter [14]. While the lattice recovers rapidly near room temperature through self-annealing—retaining only a small fraction of the original, radiation-induced defects [15,16]—the α particles acquire two electrons and remain as He atoms captured in the lattice, predominantly at lattice vacancies directly after the decay event [17,18].

During natural aging near room temperature, the vacancy-occupying He atoms (or He-filled vacancies) are mobile, capable of moving throughout the Pu matrix with a diffusive activation energy (~ 0.7 eV) associated with the occupied vacancy [19]. When two diffusing He-filled vacancies meet, a He bubble comprising two He atoms is nucleated. The driving force for this nucleation is likely provided by the energy reduction associated with the formation of a di-vacancy or the destruction of one of the original vacancies, with the latter scenario liberating significantly more energy. The nucleated He bubble will then grow through

* Corresponding Author.

Email address: jeffries4@llnl.gov (J. R. Jeffries).

this diffusive mechanism by aggregating other He-filled vacancies. This growth process is naturally limited, and He bubbles are expected to reach an equilibrium size defined by internal pressure, surface energy, and lattice yield stress. Indeed, transmission electron microscopy (TEM) observations of aged Pu-Ga alloys indicate that the distribution of He bubble diameters is narrow and strongly peaked near 1.4 nm, a value that moves little with material age between roughly 20 and 40 years [20].

Previous optical metallography experiments performed on aged Pu-Ga alloys by Wheeler and Bayer indicate that higher annealing temperatures favor an increase in He bubble diameter [21]. While the general trend of increased bubble size with increased temperature is concordant with the expected temperature-dependent evolution of the parameters controlling bubble size, it is perplexing that bubble diameters following a 500 °C/336 hr. anneal were reported to approach 60 μm , greater than four orders of magnitude larger than the equilibrium size at ambient temperature [20]. Furthermore, Wheeler and Bayer postulate, by comparison of activation energies, that bubble growth during annealing occurs via Ostwald ripening as well as an unidentified mechanism that led to the formation of large break-away bubbles. Reconciling the reported high-temperature behavior of He bubbles with those seen at ambient temperature is important to understanding the energetics associated with the aging of Pu.

In order to further elucidate the evolution of He bubbles in Pu-Ga alloys with high-temperature heat treatments, we have performed a series of annealing experiments on aged Pu-Ga alloys in the temperature range 250 °C to 450 °C using transmission electron microscopy. An increase in the average diameter and a decrease in the number density of He bubbles is observed for anneals above 375 °C. The largest average He bubble diameters, observed following a 425 °C/24 hr. anneal, are approximately 15 nm, in stark contrast to the 700-nm diameter bubbles reported by Wheeler and Bayer for a similar 400 °C/16 hr. anneal [21]. Analysis of the annealing experiments as well as *in situ* TEM observations strongly support a migration and coalescence mechanism for He bubble coarsening.

2. Experimental Details

Specimens for TEM experiments were prepared from 42- and 20-year-old Pu-3.3 at.% Ga alloys using previously reported methods [20,22,23]. After initial characterization, the samples were annealed in a vacuum furnace with the following annealing schedules: 250 °C for 2 and 24 hours (42-year-old specimen), 325 °C for 2 and 24 hours (42-year-old specimen), 375 °C for 90 hours (20-year-old specimen), and 425 °C for 2 and 24 hours (42-year-old specimen). Following the annealing treatment, the samples were returned to room temperature and examined in the TEM. Additional *in situ* annealing experiments on 42-year-old samples were performed within the TEM using a Gatan hot stage.

TEM characterization was accomplished with a Philips CM300 FEG TEM operated at 300 kV. Images were acquired using a Gatan imaging filter in combination with a CCD camera. Helium bubbles were resolved in a non-diffracting condition using the Fresnel imaging technique, which permits the observation, in the over- or under-focused condition, of strain fields associated with the otherwise irresolvable He bubbles [20]. The He bubbles in the micrographs were analyzed in ImageJ to determine the distributions of bubble diameters and bubble densities.

3. Results and Discussion

3.1. Temperature-dependent bubble properties

Example bright-field micrographs resulting from the TEM characterization are shown in Figure 1. He bubbles can be resolved as circular, white objects within the darker matrix corresponding to the Pu-Ga matrix. Figure 1a is representative of the He bubble configuration expected for the naturally aged alloys examined. Bubbles have a characteristic average size of approximately 1.4 nm and an average number density of about 94×10^{15} bubbles/ cm^3 , consistent with previously reported values for as-aged material. Additionally, Figures 1b-f show, respectively, representative micrographs for the following annealing schedules: 325 °C for 2 hrs., 325 °C for 24 hrs., 375 °C for 90 hrs., 425 °C for 2 hrs., and 425 °C for 24 hrs. Images from a 250 °C anneal look nearly identical to those corresponding to the naturally aged condition and, as such, have been excluded for brevity. The images of Figure 1 clearly show a tendency for increased bubble size and decreased bubble density with increasing annealing temperature. There was no evidence for large, micron-sized bubbles as seen by Wheeler and Bayer for comparable annealing schedules [21]. The images of Figure 1 were analyzed to determine the distributions of bubble diameter and bubble density, the values of which are given in Table 1 and shown in Fig. 2.

The parameters determined from numerous TEM images are plotted in Figure 2. The average number density of He bubbles increases slightly for 2-hr. anneals up to 250 °C, above which the number density begins to drop off with increasing anneal temperature. In the case of 24-hr. anneals, the number density of bubbles follows a similar trend to that of the 2-hr. anneals, but with tendency for lower bubble density at a given temperature. By 425 °C, the number densities from both 2- and 24-hr. anneals are comparable. The He bubbles remain near their naturally aged size for annealing temperatures up to approximately 325 °C. For annealing temperature greater than 325 °C, the average size of the He bubbles grows rapidly, increasing by nearly an order of magnitude in size between 325 °C and 425 °C for 24-hr. anneals. With increasing annealing temperature, a distinct gap in the behavior of the bubble growth begins to develop between the data for 2- and 24-hr. anneals (solid blue line vs. dashed blue line in Fig. 2).

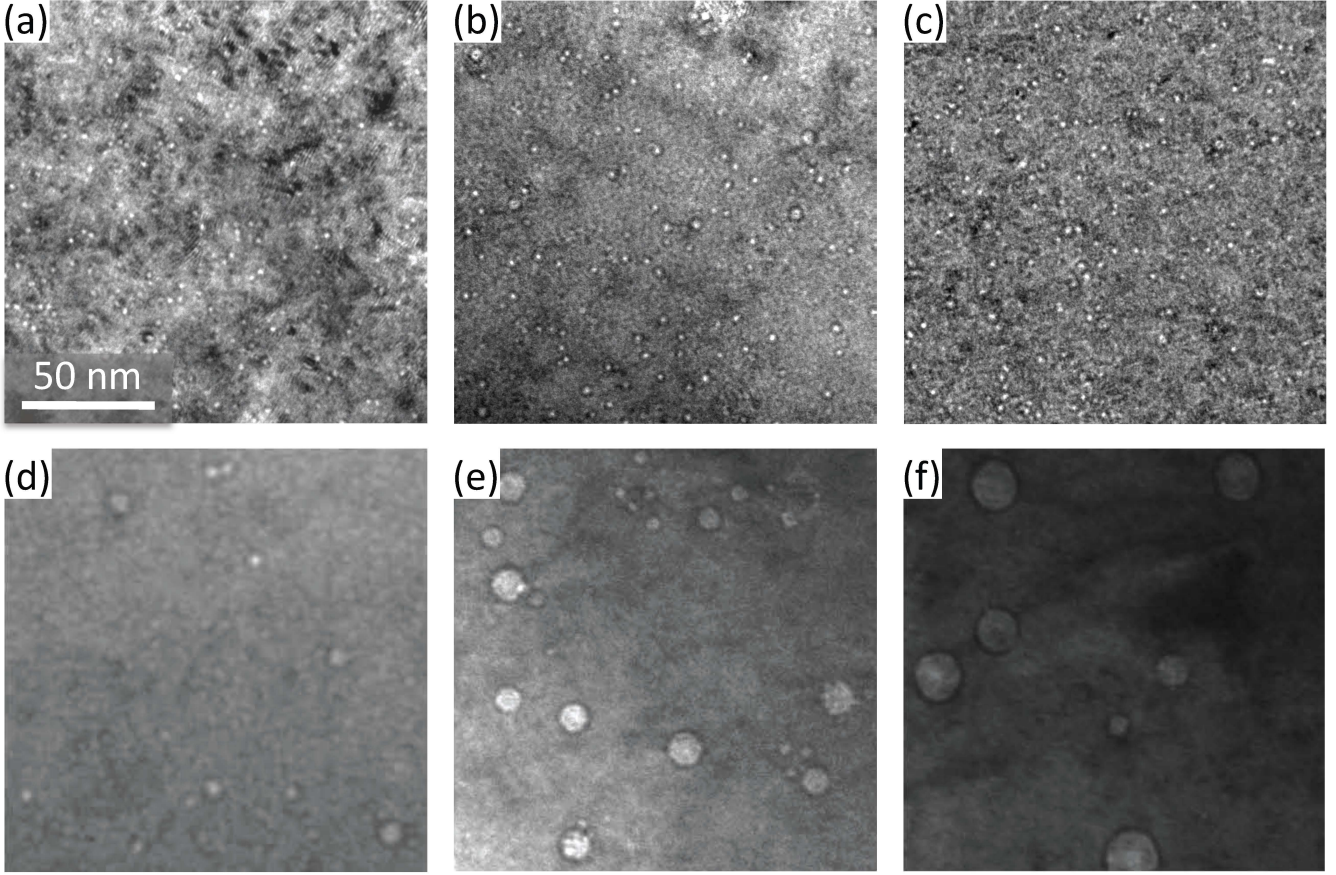


Fig. 1. Bright-field TEM micrographs of He bubbles in naturally aged and annealed Pu-Ga specimens. Each micrograph spans a 160 x 160 nm area, the scale bar is included only in (a). The He bubbles are seen as white, circular objects within the darker, grey matrix of the Pu-Ga specimen. The individual panes correspond to specimens undergoing the following annealing treatments: (a) naturally aged, (b) 325 °C for 2 hrs., (c) 325 °C for 24 hrs., (d) 375 °C for 90 hrs., (e) 425 °C for 2 hrs., and (f) 425 °C for 24 hrs.

3.2. Conservation of He residing in bubbles

Helium bubble coarsening in Pu-Ga alloys is generally thought to occur through one of two mechanisms [24]: Ost-

Table 1

He bubble parameters extracted from statistical analysis of the bubble distributions for various annealing schedules. With the exception of the naturally aged sample (Nat. Aged), the annealing schedules are given in the left column in the format of T/t , where T is the annealing temperature and t is the annealing time.

	Mean Diameter (nm)	Diameter Std. Dev. (nm)	Number Density (10^{15} cm^{-3})	Bubbles Counted
Nat. Aged	1.4	0.4	94	1378
250 °C/2 hrs.	1.3	0.4	199	2212
250 °C/24 hrs.	1.3	0.3	113	663
325 °C/2 hrs.	1.4	0.5	142	2558
325 °C/24 hrs.	1.4	0.7	90	1726
375 °C/90 hrs.	5.2	1.9	7.4	199
425 °C/2 hrs.	7.9	3.9	12.1	1179
425 °C/24 hrs.	10.9	4.4	7.3	371

wald ripening (OR)—wherein larger bubbles expand at the expense of smaller bubbles, with individual He atoms diffusing through the lattice from small to large bubble [25]; and bubble migration and coalescence (MC)—wherein bubbles move through the lattice via surface diffusion, and grow by coalescing during collisions with one another [26]. In the latter case, MC, the amount of He residing in bubbles must be conserved, as He does not exit the confines of a bubble during collisions. In the former case, He atoms do leave the confines of the bubble, but may do so in a small, nearly undetectable quantity. As such, it is difficult to rule out the possibility of an OR mechanism simply by examining, through TEM micrographs, whether the number of He atoms residing in bubbles is conserved. However, for MC to be a valid mechanism for bubble coarsening in Pu-Ga alloys, the amount of He residing in bubbles *must* be conserved.

If the number of He atoms residing in bubbles is conserved, then the bubble number density and average bubble diameter are intimately linked by the total He content of the system, \mathcal{N}_{He} . Accounting for the He atoms in bubbles takes the form of:

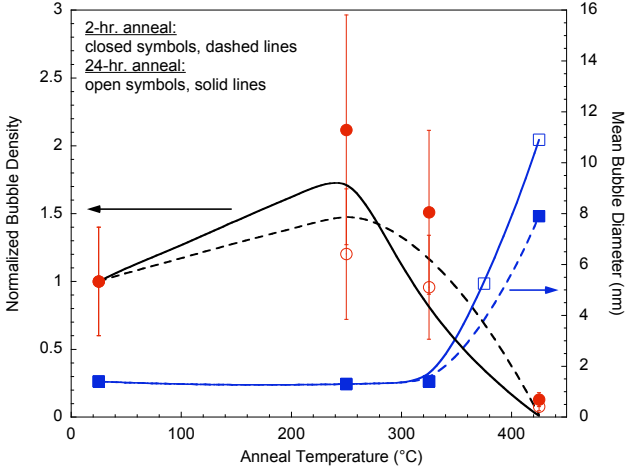


Fig. 2. Measured (red, closed or open circles, left axis) and calculated bubble density (black, dashed or solid lines, left axis) normalized to the naturally aged value and mean bubble diameter (blue symbols, right axis) as functions of annealing temperature. Data and calculations corresponding to 2-hr. anneals are shown as closed symbols connected with dashed lines, while 24-hr. anneals are represented by open symbols connected with solid lines. The data point for the bubble diameter at 375 °C was determined after a 90 hr. anneal. The blue lines are smooth fits to the bubble diameter data, while the black lines represent bubble densities calculated from the bubble size distributions in accord with the conservation of He (see text).

$$\mathcal{N}_{He} = \sum_r N_{He}^B(r) n_r^B,$$

where $N_{He}^B(r)$ is the number of He atoms within a bubble of radius r , n_r^B is the number of bubbles having radius r , and the summation is over all r . Each one of these parameters is continuous, yielding an integral equation:

$$\mathcal{N}_{He} = \int_0^r N_{He}^B(r) n_r^B dr. \quad (1)$$

According to analysis of the TEM micrographs, the number of bubbles with radius r is reasonably well represented by a Gaussian:

$$n_r^B = \frac{\mathcal{H}}{\sqrt{2\pi}\sigma} e^{-\frac{(r-r_M)^2}{2\sigma^2}}, \quad (2)$$

where r_M is the mean value of the bubble radius, σ is the standard deviation of the distribution of bubble radii, and \mathcal{H} is a constant scaling the height of the distribution.

The number of He atoms within a bubble of radius r can be expressed as:

$$N_{He} = \frac{4}{3}\pi\rho_A r^3, \quad (3)$$

where ρ_A is the volumetric He number density (*i.e.*, number of helium atoms per unit volume) and the volume of the bubble is assumed to be that of a sphere. The number density of He atoms within a bubble is related to the bubble pressure, P_B , and temperature, T . Because the anneal temperatures and bubble pressures are far in excess of the critical temperature and pressure of He, the ideal gas law

can elicit large errors in the determination of the He number density. Instead, we use the Virial equation of state:

$$\frac{P_B}{k_B T} = \rho_A + \sum_{j=2}^{\infty} B_j \rho_A^j,$$

where k_B is Boltzmann's constant and B_j are the j^{th} Virial coefficients, each of which can be a function of temperature. Here, we truncate the Virial equation of state after $j = 2$, yielding a quadratic equation:

$$\frac{P_B}{k_B T} = \rho_A + B_2(T) \rho_A^2, \quad (4)$$

which approaches the ideal gas law in the limit as B_2 approaches zero. Ignoring the negative solution to Eq. 4, the He number density can then be expressed as:

$$\rho_A(T, P) = \frac{1}{2B_2(T)} \left[\sqrt{1 + \frac{4B_2(T)P_B}{k_B T}} - 1 \right]. \quad (5)$$

Between 200 and 350 K, B_2 for He is positive and weakly temperature dependent, linearly decreasing only slightly with increasing temperature [27]. This temperature dependence can be extrapolated by a line:

$$B_2(T) = 12.612 - 0.005T, \quad (6)$$

where B_2 is given in units of cm^3/mole .

The pressure inside a He bubble is a function of the bubble radius [8]:

$$P_B(r) = \frac{2}{3}\sigma_y + \frac{2\gamma}{r}, \quad (7)$$

where σ_y is the yield stress of the metal matrix and $\gamma \approx 1.4 \times 10^{-4} \text{ J/cm}^2$ is the surface tension of the bubble-matrix interface that gives rise to the interfacial energy of the bubble. The yield stress of δ -Pu is temperature dependent, and, for a specimen with comparable Ga content and preparation, has been reported to be linear with [28]:

$$\sigma_y = 1378.4 - 1.9T,$$

where σ_y is given in bar and calculated using T in kelvin.

Combining the above formulae, Eq. 1 can be expressed as a function of r :

$$\mathcal{N}_{He}(T) = \frac{4\pi\mathcal{H}}{6\sqrt{2\pi}\sigma} \frac{1}{B_2} \int_0^r \left[\sqrt{1 + \frac{4B_2 P_B(r)}{k_B T}} - 1 \right] \times r^3 e^{-\frac{(r-r_M)^2}{2\sigma^2}} dr. \quad (8)$$

(N.B. the explicit temperature dependence of B_2 has been suppressed in Eq. 8, but B_2 should be considered a temperature-sensitive quantity). The values of r_M and σ are implicitly temperature dependent, but the value of \mathcal{N}_{He} is conserved regardless of annealing temperature or time. This means that given a bubble distribution corresponding to an annealing temperature, He conservation is

manifested through the bubble size distribution parameter \mathcal{H} .

With increasing annealing temperature, the evolution of the parameter \mathcal{H} is evidenced in the corresponding evolution of the He bubble density, D_B , which is defined from the bubble radius distribution as the total number of bubbles in the system, N_B , divided by the system volume:

$$D_B = \frac{N_B}{V} = \frac{1}{V} \int_0^r \frac{\mathcal{H}}{\sqrt{2\pi}\sigma} e^{-\frac{(r-r_M)^2}{2\pi\sigma^2}} dr. \quad (9)$$

As He bubbles coarsen with increasing annealing temperature, the bubble size distribution evolves, dictating that the He bubble density respond accordingly through the shared dependence of \mathcal{N}_{He} and D_B upon \mathcal{H} . As the bubble size distribution shifts to higher bubble radius, the amount of He contained in each bubble increases (driven by the volume increase), and the magnitude (height \mathcal{H}) of the bubble size distribution must decrease in order to obey the conservation of He. The decrease in the magnitude of the bubble size distribution yields a decrease in the He bubble density.

This inverse relationship between average bubble size and bubble density can be seen in Fig. 2, where the solid and dashed black lines represent bubble densities calculated from the measured radius distributions by use of Eq. 8. The bubble density measurements (red symbols) bear out the general trend expected for the evolution of the bubble density calculated from the size distributions, and the discrepancies between the calculations and observations are certainly within error. Unfortunately, the error associated with extracting the bubble density from the TEM micrographs is relatively large. The TEM micrographs look through a volume of sample, therefore there is an error associated with undercounting bubbles that may be occulted by bubbles above. Furthermore, there is a substantial error in estimating the volume under examination. These errors lead to an uncertainty in the bubble density of at least 30%, with the majority of the uncertainty deriving from the error in the volume estimate.

While it appears from Fig. 2 that the amount of He residing in bubbles is likely conserved, supporting MC as a mechanism, OR cannot be excluded due to the error associated with the bubble density measurement. Given the large error in the measurements of bubble density, both prevailing mechanisms for bubble coarsening, OR and MC, remain plausible.

3.3. Time-dependent bubble observations

A fundamental difference between bubble coarsening through MC and OR is the mobility of the bubble within the Pu matrix. Because an OR mechanism transfers He from small to large bubbles via He diffusion through the lattice, the center of mass of the bubble is not expected to move as the bubble changes size (*i.e.*, loses or gains He). On the contrary, a MC mechanism requires that the center of mass of the bubbles move through the Pu ma-

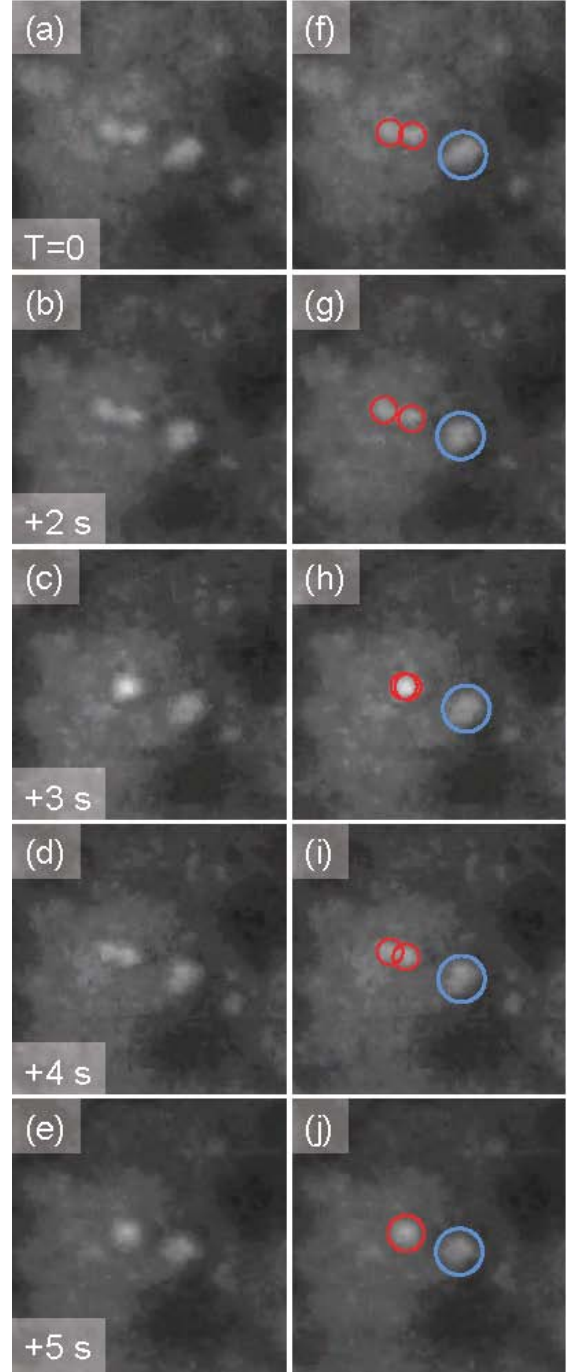


Fig. 3. Bright-field, *in situ* TEM micrographs of He bubble evolution as a function of time in a naturally aged Pu-Ga specimen at 450 °C. Panels (a)-(e) show the time-dependent motion of the He bubbles over a 5 second window. Bubbles of interest in (a)-(e) are marked by circles in the neighboring panels (f)-(j). Bubble coalescence is clearly visible in panels (e) and (j), where the two bubbles marked by red circles are no longer discernible, the strain field is symmetric, and the diameter of the strain field is increased.

trix. This qualitative difference between MC and OR is a time-dependent phenomenon, therefore a time-resolved measurement must be used to distinguish between the two mechanisms of coarsening.

Time-resolved TEM micrographs show clear evidence of

large-scale bubble migration (see Supplementary Online Materials for videos), a necessary component of MC. The bubbles appear to move randomly within the lattice, reminiscent of Brownian motion of bubbles seen in other FCC metals [29]. Bubbles can also pin on dislocations, ceasing to be mobile for extended periods of time, as well as become unpinned, regaining mobility within the matrix. Figure 3 displays a series of time-resolved bright-field TEM micrographs of a Pu-Ga alloy at 450 °C. A clear signature of bubble coalescence is captured in this series of images.

The left column of Fig. 3, panels (a)-(e), shows the evolution of several bubbles as a function of relative time steps, denoted in the bottom left corner of each panel. The right column of Fig. 3, panels (f)-(j), are identical to the left column except for the circles labeling the positions of the three specific bubbles. The right-most, blue circle denotes a pinned bubble (approximately 7 nm in diameter), which does not move with time and serves as an effective fiducial point. This pinned bubble is likely collocated with a defect that prevents surface diffusion. To the left of the pinned bubble are two bubbles (each about 3.8 nm in diameter), circled with two red circles in panels (f)-(j), that coalesce 5 seconds after the first image.

Within the first 2 seconds, the two mobile bubbles appear to move away from each other, but then appear to coalesce (Figs. 3c and h) after 3 seconds. However, one can see that the strain field associated with the two bubbles is slightly asymmetric, indicating that the bubbles are nearly aligned in the horizontal image plane but offset along the vertical direction. After 4 seconds, the bubbles are clearly separate (Figs. 3d and i), and, finally, after 5 seconds, the two bubbles have coalesced into a single bubble (Figs. 3e and j). The strain field identifying the bubble is clearly symmetric, and the bubble diameter is approximately 42% larger (5.4 nm in diameter) than the original bubbles, in excellent agreement with the expected bubble diameter (5.2 nm) calculated using the equations of Section 3.2.

4. Conclusions

In naturally aged Pu-Ga alloys, annealing at elevated temperatures between 325 and 450 °C causes coarsening of the He bubble distribution, decreasing the overall number density of bubbles and increasing the average size of the He bubbles. There is a time and temperature dependence to the bubble coarsening, with longer times and higher anneal temperatures both having the effect of reducing the bubble density and increasing the mean bubble size. Analysis of TEM micrographs subsequent to annealing treatments is consistent with the conservation of He residing in the He bubbles—which supports coarsening through MC, but, due to the magnitude of measurement errors, does not exclude OR as a coarsening mechanism. Time-resolved, *in situ* TEM micrographs, however, clearly evince both bubble migration and coalescence, leading to the conclusion that MC is the primary mechanism by which He bubbles

coarsen in Pu-Ga alloys at these temperatures.

5. Acknowledgments

This work was supported by the Science Campaign at Lawrence Livermore National Laboratory. Lawrence Livermore National Laboratory is operated by Lawrence Livermore National Security, LLC, for the U.S. Department of Energy, National Nuclear Security Administration under Contract DE-AC52-07NA27344.

References

- [1] H. Trinkaus, J. Nucl. Mater. **133&134**, 105 (1985).
- [2] H. Trinkaus and B. N. Singh, J. Nucl. Mater. **323**, 229 (2003).
- [3] H. Trinkaus, Scripta Metall. **23**, 1773 (1989).
- [4] S. E. Donnelly, Radiat. Eff. **90**, 1 (1985).
- [5] R. C. Birtcher, S. E. Donnelly, and C. Templier, Phys. Rev. B **50**, 764 (1994).
- [6] A. Arsenlis, W. G. Wolfer, and A. J. Schwartz, J. Nucl. Mater. **336**, 31 (2005).
- [7] R. J. M. Konings, T. Wiss, and C. Guéneau, In: N. M. Edelstein, J. Fuger, and L. R. Morss (Eds.), The Chemistry of the Actinide and Transactinide Elements (Volume 6), Springer; 2010. Ch. 34.
- [8] P. G. Klemens and B. Cort, J. Alloys Compd. **252**, 157 (1997).
- [9] S. I. Golubov, R. E. Stoller, S. J. Zinkle, and A. M. Ovcharenko, J. Nucl. Mater. **361**, 149 (2007).
- [10] S. S. Hecker, Metall. Mater. Trans. A **39A**, 1585 (2008).
- [11] K. T. Moore and G. van der Laan, Rev. Mod. Phys. **81**, 235 (2009).
- [12] A. J. Schwartz, H. Cynn, K. J. M. Blobaum, M. A. Wall, K. T. Moore, W. J. Evans, D. L. Farber, J. R. Jeffries, and T. B. Massalski, Prog. Mater. Sci. **54**, 909 (2009).
- [13] W. G. Wolfer, Los Alamos Sci. **26**, 274 (2000).
- [14] A. Kubota, W. G. Wolfer, S. M. Valone, and M. I. Baskes, J. Comput-Aid. Mater. Des. **14**, 367 (2007).
- [15] M. J. Fluss, B. D. Wirth, M. A. Wall, T. E. Felter, M. J. Caturla, A. Kubota, and T. D. de la Rubia, J. Alloys Compd. **368**, 62 (2004).
- [16] S. K. McCall, M. J. Fluss, B. W. Chung, M. W. McElfresh, G. F. Chapline, D. D. Jackson, and R. G. Haire, J. Alloys Compd. **444-445**, 168 (2007).
- [17] R. H. Howell, P. A. Sterne, J. Hartley, and T. E. Cowan, Appl. Surf. Sci. **149**, 103 (1999).
- [18] S. M. Valone, M. I. Baskes, and R. L. Martin, Phys. Rev. B **73**, 214209 (2006).
- [19] B. D. Wirth, A. J. Schwartz, M. J. Fluss, M. J. Caturla, M. A. Wall, and W. G. Wolfer, MRS Bull. **26**, 679 (2001).
- [20] A. J. Schwartz, M. A. Wall, T. G. Zocco, and W. G. Wolfer, Phil. Mag. **85**, 479 (2005).
- [21] D. W. Wheeler and P. D. Bayer, J. Alloys Compd. **444-445**, 212 (2007).
- [22] K. T. Moore, M. A. Wall, and A. J. Schwartz, J. Nucl. Mater. **306**, 212 (2002).
- [23] K. T. Moore, Micron **41**, 336 (2010).
- [24] H. Schroeder and P. F. P. Fichtner, J. Nucl. Mater. **179-181**, 1007 (1991).
- [25] A. Baldan, J. Mater. Sci. **37**, 2171 (2002).
- [26] E. E. Gruber, J. Appl. Phys. **38** 243 (1967).
- [27] J. G. Kirkwood and F. G. Keyes, Phys. Rev. **37**, 832 (1931).
- [28] J. L. Robbins, J. Nucl. Mater. **321**, 125 (2004).
- [29] K. Ono, K. Arakawa, K. Hojou, M. Oohasi, R. C. Birtcher, and S. E. Donnelly, J. Electron. Microsc. **51**, S245 (2002).